Check for updates

ChemSusChem

Research Article
doi.org/10.1002/cssc.202500267

Chemistry Europe
European Chemical Societies Publishing

www.chemsuschem.org

Carbon-Coated Silver Nanoparticles for Highly Robust Chloride Capture in Electrochemical Desalination and Lithium Recovery

Seoni Kim,* Sung Pil Hong, Hwajoo Joo, Chanhyeong Lee, Yung-Eun Sung, Jeyong Yoon,* and Jin Soo Kang*

In recent years, electrochemical desalination and resource recovery processes have gained significant attention as means of utilizing waters, wherein the majority of anionic species are chloride ions. There have been research efforts to develop high-performance electrode materials for the chloride uptake. Silver with extremely fast kinetics is an ideal option, but the cost and stability issues are yet to be resolved. Herein, silver nanoparticles with nitrogen-doped carbon (NC) shells are developed for electrochemical Cl^- capture in desalination and lithium recovery processes. Starting from commercial Ag powders, nanosized particles are obtained by the chlorination to AgCl, which is followed by the polydopamine coating and thermal annealing. Interestingly, dopamine polymerization can be coupled with the dechlorination of the AgCl, enabling the simultaneous polymeric shell formation and AgCl-to-Ag conversion. This NC-coated Ag nanoparticles (N-Ag@NC) manifest superior capacity and cyclic stability in electrochemical Cl^- capture, when compared with those of Ag particles without NC shells or with a larger (microscale) size. The enhanced performance is attributable to the small particle sizes and the NC shells, which result in a higher Ag utilization and tolerance to the volume changes accompanying the chlorination/dechlorination.

1. Introduction

Water on our planet's surface, including both seawater and brackish water, is one of the largest reservoirs of various essential resources, ranging from water for intake and residential purposes to valuable elements existing as ionic species.[1,2] Purification of water or extraction of useful components is often important to maximize the value of water resources. Conventional water treatment processes such as thermal distillation, membrane process, adsorption, and precipitation are based on highly mature technologies,[3–6] while electrochemical methods have been widely investigated recently.[7–9] Advances of electrode materials that can capture ions either by adsorption on the electrified surface or by Faradaic insertion enabled deionization of saline water and recovery of resources using electrochemical systems.[9–12] Electrochemical techniques have gained significant attention owing to their environmentally benign features (unlike most of the conventional processes) and for directly using electricity as

S. Kim
Department of Environmental Science and Engineering
Ewha Womans University
Seoul 03760, Korea
E-mail: seonikim@ewha.ac.kr

S. Kim, S. P. Hong, H. Joo, Y.-E. Sung, J. Yoon
School of Chemical and Biological Engineering and Institute of Chemical Processes (ICP)
Seoul National University
Seoul 08826, Korea
E-mail: jeyong@snu.ac.kr

C. Lee, J. S. Kang
Department of Energy Systems Engineering
Seoul National University
Seoul 08826, Korea
E-mail: jinsookang@snu.ac.kr

Y.-E. Sung, J. S. Kang
Center for Nanoparticle Research
Institute for Basic Science (IBS)
Seoul 08826, Korea

J. Yoon, J. S. Kang
SNU Energy Initiative
Seoul National University
Seoul 08826, Korea

J. S. Kang
Department of Energy Resources Engineering and Research Institute of Energy and Resources
Seoul National University
Seoul 08826, Korea

J. S. Kang
Institute for Battery Research Innovation
Seoul National University
Seoul 08826, Korea

Supporting information for this article is available on the WWW under https://doi.org/10.1002/cssc.202500267

© 2025 The Author(s). ChemSusChem published by Wiley-VCH GmbH. This is an open access article under the terms of the Creative Commons Attribution-NonCommercial-NoDerivs License, which permits use and distribution in any medium, provided the original work is properly cited, the use is non-commercial and no modifications or adaptations are made.

© 2025 The Author(s). ChemSusChem published by Wiley-VCH GmbH

the energy source (i.e., potentially compatible with renewable energy sources).[13–15]

Among various approaches, capacitive deionization, desalination battery, and electrochemical lithium recovery are typical examples of electrochemical techniques with high feasibility and reliability.[13,15–19] In these desalination and recovery processes, cations of interest vary depending on the targeted application or product. On the other hand, the majority of anions in source waters is chloride ion (Cl^-). For this reason, there have been significant efforts to develop high-performance electrode materials for chloride uptake.[9] As the selectivity of the electrode toward Cl^- is often an insignificant issue, materials with large surface areas have been used extensively, capturing chloride by capacitive or pseudocapacitive reactions.[20–24] However, non-Faradaic electrodes generally have relatively small capacities, and thus, Faradaic materials were also investigated to increase the Cl^--capture amounts.[25–29]

Among the well-known materials that undergo Faradaic reactions with Cl^-, silver shows incomparably faster kinetics in chlorination and (following) dechlorination.[9,30,31] This means that Ag is the electrode material with the lowest overpotential and energy consumption during the Cl^- capture and release. Despite the advantages in energetics, high cost, and insufficient long-term stability often limit the application of silver electrodes.[31,32] To resolve these issues, there have been diverse attempts to maximize the utilization of silver and retain the performance during the cyclic operations. For instance, compositing silver particles with *m*-phenylenediamine-derived heteroatom-doped carbon led to high chloride-capture capacities, which were attributed to favorable Ag-C configurations and the strong interaction between Ag and the heteroatom dopants.[33–36] Embedding Ag particles in MXene, metal–organic framework-derived carbon, or holey carbon aerogels also showed decent performances.[37–39] However, these materials and their synthesis procedures are usually not feasible for large-scale applications.

In this study, silver nanoparticles with a nitrogen-doped carbon (NC) shell on the surface were prepared for highly robust capture and release of Cl^-. Starting from commercially available micrometer-scale Ag particles, nanosizing and carbon-coating were performed by chlorination of Ag (using $FeCl_3$) and formation of polydopamine shell, followed by thermal annealing, respectively. Meanwhile, it was noteworthy that the favorable redox potentials of the dopamine polymerization processes enabled the simultaneous dechlorination and coating of Ag, which not only simplified the synthesis procedures but also facilitated the polymerization reaction. When the synthesized Ag nanoparticles with NC shells were applied for chloride capture in electrochemical desalination and lithium recovery, they manifested excellent performances in terms of both capacity and stability during the long-term chlorination/dechlorination cycles. With the assistance of various characterization techniques, we could ascribe the robustness to the structural characteristics of the particles, including the nanosize that reduces the overall strain caused by the volume change and the presence of carbonaceous shells that serve as a protective layer and conductive matrix throughout the operations.

2. Results and Discussion

The synthesis of carbon-coated silver nanoparticles was performed by using commercial silver powders whose sizes were within the micrometer scale. As depicted in the schematic illustration (**Figure 1**), microsized silver particles (M-Ag) were chlorinated by dispersing 1 g of M-Ag in 250 mL of an aqueous solution containing 40 mM of polyvinylpyrrolidone as the surfactant, followed by dropwise addition of iron chloride hexahydrate solution (1.92 g $FeCl_3{\cdot}6H_2O$ in deionized water, total volume: 50 mL). Chlorination of silver could take place by the coupling of the following reactions.[40]

$$Fe^{3+}(aq) + e^- \rightarrow Fe^{2+}(aq)\ (E^0 = +0.77\,V\,vs.\,NHE) \quad (1)$$

$$Ag\,(s) + Cl^-(aq) \rightarrow AgCl\,(s) + e^-(E^0 = +0.22\,V\,vs.\,NHE) \quad (2)$$

where NHE stands for normal hydrogen electrode. The resulting particles obtained after filtration were named as nanosized AgCl (N-AgCl), of which the materials characterization results are introduced in the following paragraphs. We carried out the polydopamine coating of M-Ag and N-AgCl by dispersing them in 300 mL of aqueous phosphate buffer (200 mM, pH 8.5–9) under stirring, and 300 mg of dopamine hydrochloride was added to the solution. After stirring the solution for 24 h, polydopamine-coated particles were produced.

The chlorinated and polydopamine-coated particles were characterized by X-ray diffraction (XRD) measurements using a synchrotron radiation source. From the XRD patterns shown in **Figure 2**, it was clearly observed that the chlorination of M-Ag was successfully carried out, while there was some remaining metallic Ag in the N-AgCl. It was noteworthy that the polydopamine-coated samples (marked with @PD) appeared to be metallic Ag in the XRD results, without any signal from AgCl, even in the case of the coated N-AgCl. This indicates that dechlorination of AgCl occurs during the coating process of N-AgCl, and we hereafter note that the polydopamine-coated particles as M-Ag@PD and N-Ag@PD with regards to their sizes and compositions.

In order to understand the observed in situ dechlorination during the polydopamine coating, we investigated the polymerization mechanism of dopamine monomers.[41–43] As displayed in **Figure 3**, this process includes multiple chemical and electrochemical reaction steps, which are marked with C and E (with numbers in ascending order), respectively. It is widely known that E1 and E2 are oxidation reactions that can take place by coupling with the oxygen reduction reaction, and the presence of O_2 is, therefore, highly important for the polydopamine coating process. Meanwhile, oxidation of dopamine to dopaminequinone (E1) occurs at the potential below Ag/AgCl at mild pH conditions, including the phosphate buffer, wherein the dopamine polymerization was carried out. Therefore, it is possible for E1 to be coupled with the reduction of AgCl (to Ag), which would also facilitate the polymerization of dopamine at the particle surface. This seems to be the most probable reason for the observed in situ dechlorination of AgCl during the coating of N-AgCl.

M-Ag@PD and N-Ag@PD were thermally annealed in N_2 atmosphere at 150 °C for 1 h, followed by 500 °C for 4 h; this

© 2025 The Author(s). ChemSusChem published by Wiley-VCH GmbH

1864564x, 2025, 16, Downloaded from https://chemistry-europe.onlinelibrary.wiley.com/doi/10.1002/cssc.202500267 by Ewha Womans University Library, Wiley Online Library on [02/12/2025]. See the Terms and Conditions (https://onlinelibrary.wiley.com/terms-and-conditions) on Wiley Online Library for rules of use; OA articles are governed by the applicable Creative Commons License

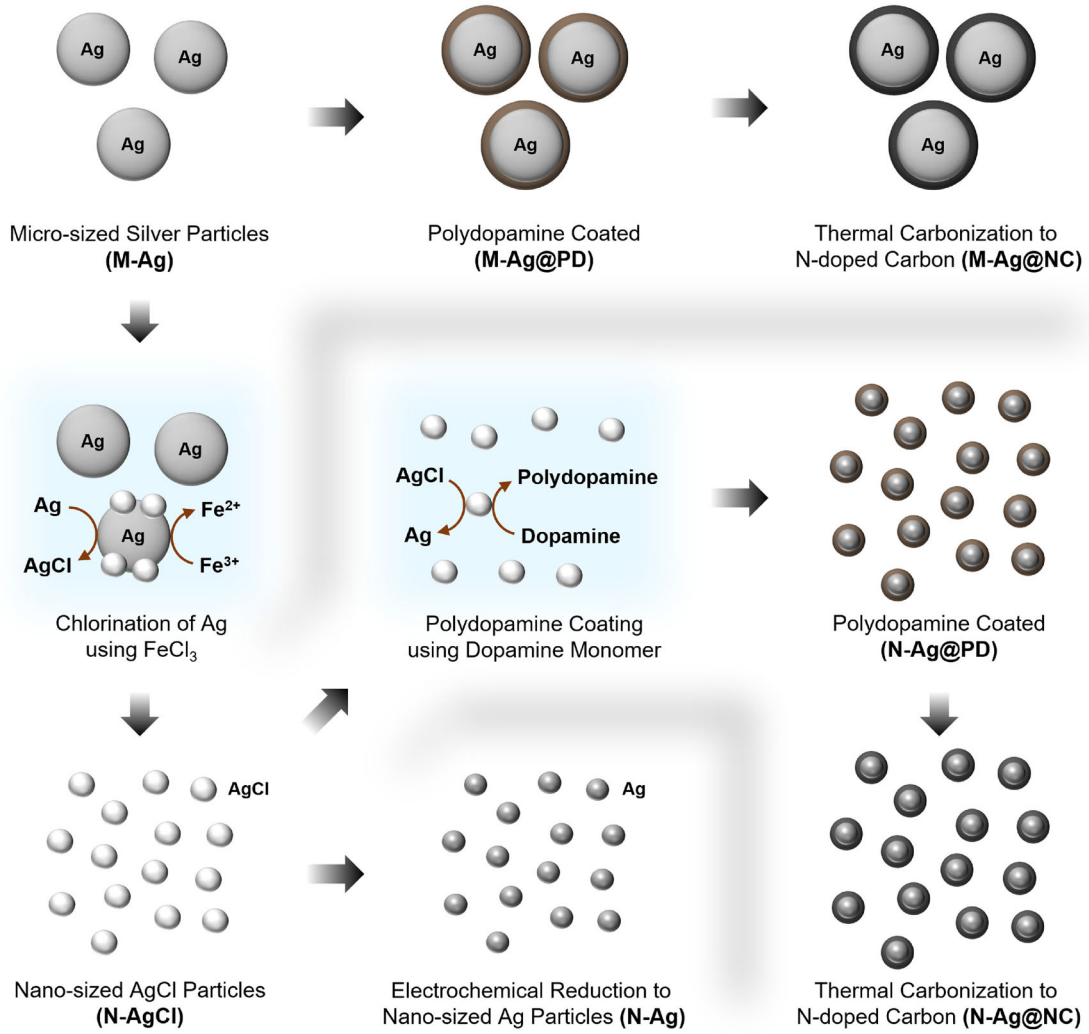


Figure 1. Schematic illustrations showing the processes for preparing various silver particles used for the chloride capture.

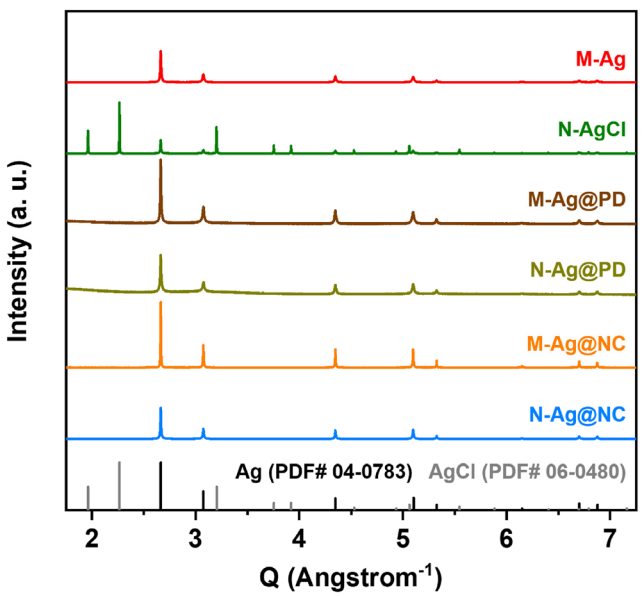


Figure 2. High-resolution XRD patterns of the silver particles. The bars at the bottom show the reference scattering vector (Q) positions of Ag (PDF# 04-0783) and AgCl (PDF# 06-0480).

elevated-temperature treatment was to turn the polydopamine layer into the NC. The carbonization of the coated layer was corroborated by the synchrotron-based high-resolution X-ray photoelectron spectroscopy (XPS) C 1*s* and N 1*s* spectra displayed in Figure S1, Supporting Information. In the case of pristine polydopamine, multiple peaks originating from C—O/C—N (≈286 eV) and C═O/C═N (≈288 eV) are observable from the C 1*s* spectrum,[44] and a broad N 1*s* peak that corresponds to the signals from N—H/N—C appears in the N 1*s* spectrum.[45] Meanwhile, the XPS spectra obtained after the thermal annealing showed the responses of N-doped amorphous carbon, especially in the case of N 1*s* spectra with the characteristic shape of combined signals from pyridinic, pyrrolic, and graphitic nitrogens.[45–47] The heat-treated particles were named as M-Ag@NC and N-Ag@NC with respect to their sizes (Figure 1). The XRD (Figure 2) and XPS (Figure S2, Supporting Information) analysis results revealed that they are composed of metallic Ag (Figure 2). Thermogravimetric analysis (TGA) of the annealed samples revealed that the relative amounts of carbonaceous species were around 12 wt% and 31 wt% in M-Ag@NC and N-Ag@NC, respectively (Figure S3, Supporting Information). This could be understood as the result

© 2025 The Author(s). ChemSusChem published by Wiley-VCH GmbH

1864564x, 2025, 16, Downloaded from https://chemistry-europe.onlinelibrary.wiley.com/doi/10.1002/cssc.202500267 by Ewha Womans University Library, Wiley Online Library on [02/12/2025]. See the Terms and Conditions (https://onlinelibrary.wiley.com/terms-and-conditions) on Wiley Online Library for rules of use; OA articles are governed by the applicable Creative Commons License

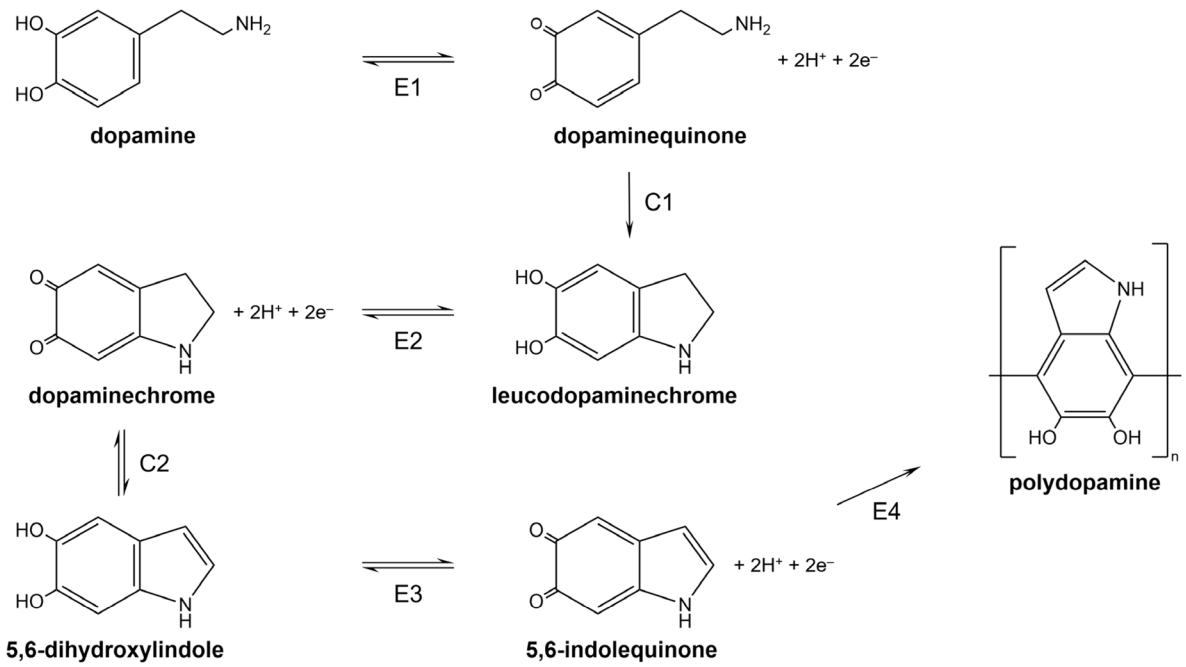


Figure 3. Mechanism of polydopamine formation by the polymerization of dopamine monomers. C and E with the numbers in ascending order indicate chemical and electrochemical reactions, respectively.

of a larger surface area in the case of nanosized particles, on which the polydopamine coating takes place. There was no significant difference in the shell thickness of M-Ag@NC and N-Ag@NC, which could be observed by the electron microscope images shown in **Figure 4**. We additionally carried out Brunauer–Emmett–Teller (BET) analysis on the NC-coated silver particles (Figure S4, Supporting Information), which gave specific the surface areas of 2.96 and 32.20 $m^2 g^{-1}$ for M-Ag@NC and N-Ag@NC, respectively.

For the electrochemical capture and release of chloride ions, we selected four samples as the electrode materials, considering the difference in their size (micro- or nano-) and existence/absence of the NC shell; the set of materials was M-Ag, nanosized Ag nanoparticles (N-Ag), M-Ag@NC, and N-Ag@NC. For the preparation of N-Ag, we first made the electrodes using N-AgCl (based on the procedures explained in the following paragraph) and performed galvanostatic dechlorination by applying -0.2 A g^{-1} (normalized by the weight of AgCl) until the electrode potential reached -0.2 V versus Ag/AgCl. Figure 4 shows the scanning electron microscopy (SEM) and transmission electron microscopy (TEM) images of M-Ag, N-Ag, M-Ag@NC, and N-Ag@NC. In

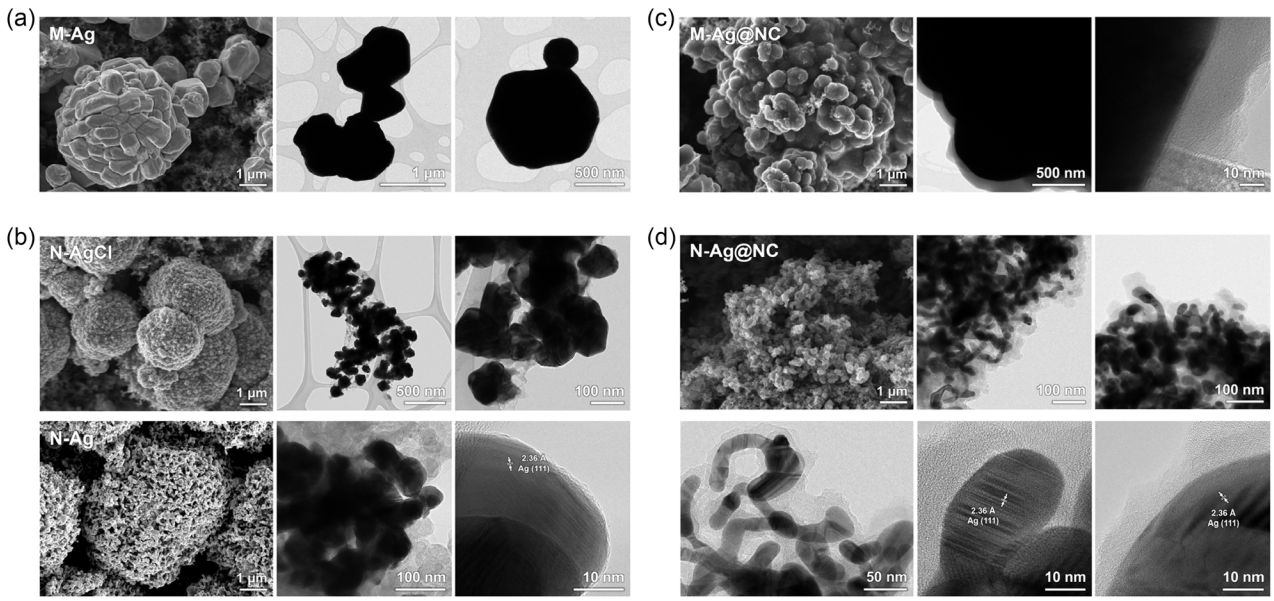


Figure 4. SEM and TEM images of silver particles used for the chloride capture. a) M-Ag, b) N-AgCl and N-Ag (prepared by electrochemically dichlorination of N-AgCl), c) M-Ag@NC, and d) N-Ag@NC.

© 2025 The Author(s). ChemSusChem published by Wiley-VCH GmbH

1864564x, 2025, 16, Downloaded from https://chemistry-europe.onlinelibrary.wiley.com/doi/10.1002/cssc.202500267 by Ewha Womans University Library, Wiley Online Library on [02/12/2025]. See the Terms and Conditions (https://onlinelibrary.wiley.com/terms-and-conditions) on Wiley Online Library for rules of use; OA articles are governed by the applicable Creative Commons License

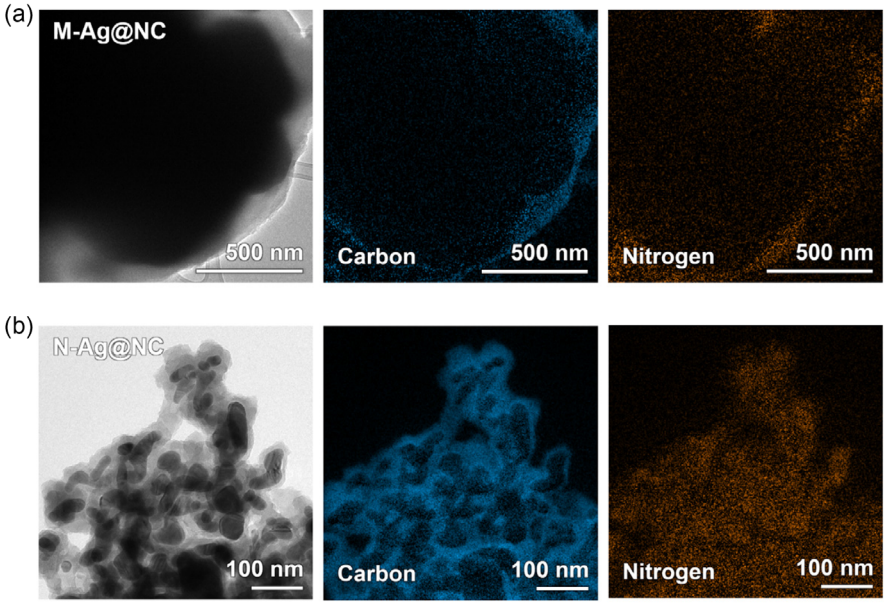


Figure 5. TEM images and the corresponding EF-TEM images showing the distribution of carbon and nitrogen in a) M-Ag@NC and b) N-Ag@NC.

addition, energy-filtered (EF)-TEM images of M-Ag@NC and N-Ag@NC clearly support the existence of NC shells on the surface (**Figure 5**). Moreover, the above-mentioned in situ dechlorination of N-AgCl during the polydopamine coating could be cross-checked by the TEM-based energy-dispersive X-ray spectroscopy analysis (Figure S5, Supporting Information), which unveiled that the atomic Ag-to-Cl ratio increased after the coating (from 3.9 to 64).

The electrodes were prepared by doctor-blading the slurry, which is composed of active materials (various silver particles), conducting agents (super P), and polymeric binder (polyvinylidene fluoride) in the ratio of 8:1:1 (by weight), on a conductive substrate (graphite sheet). In order to investigate the electrochemical behaviors of the silver particles in Cl^- capture and release, we performed cyclic voltammetry (CV) analysis. The measurements were carried out in a three-electrode configuration, using an activated carbon composite counter electrode and an Ag/AgCl (sat. KCl) reference electrode. Aqueous solution containing 1 M NaCl was used as the electrolyte, targeting the evaluation of desalination performance. From the CV curves (Figure S6, Supporting Information), it was clear that all electrodes have highly reversible Cl^- capture/release capabilities, while there seemed to be differences in kinetics. For instance, the existence of carbonaceous shell led to a significant increase in kinetics, which is attributable to the improved electrical conductivity. Electrochemical impedance spectroscopy (EIS) results shown in Figure S7, Supporting Information, corroborate the increased conductivity by smaller series resistance (R_s, corresponds to the x-intercept of the Nyquist plot). Moreover, though the sizes of the semicircles were difficult to be quantified, comparison at the high-frequency region suggests that the charge-transfer resistance (R_{ct}) is the smallest in the case of N-Ag@NC. Meanwhile, the formation of nonconductive AgCl is inevitable during the operation, and the NC shells can serve as conductive channels even at the highly-chlorinated state. It was also interesting to see that there were generally larger overpotentials for Cl^- capture compared to the release, in all four electrodes. This could be understood based on the different mechanisms of the two reactions; the mass transfer property of Cl^-, which is a key reactant, significantly affects the overall kinetic of Ag chlorination, while the AgCl dechlorination is hardly influenced by the mass transfer of reactants. This results in prompter kinetics for the dechlorination reaction, showing a smaller overpotential from the thermodynamic onset (0 V vs. Ag/AgCl).

Figure 6a–d shows the charge–discharge profiles of M-Ag, N-Ag, M-Ag@NC, and N-Ag@NC obtained under the three-electrode configuration (with the components identical to those for the CV measurements). The potential window was −0.2 to +0.2 V versus Ag/AgCl, and the operation current densities were $\pm 0.2\ A\ g^{-1}$ (normalized by the mass of active materials, including that of N-doped carbon shells). When the reaction potential was compared between the Ag particles with similar sizes (e.g., M-Ag vs. M-Ag@NC and N-Ag vs. N-Ag@NC), it was noteworthy that the overpotential for the chlorination reaction was larger for the silver with the N-doped carbon shells. On the other hand, there was no significant overpotential for the dechlorination of AgCl, and the reaction potentials were near 0 V versus Ag/AgCl for all cases. This could be explained by the difference in the rate of Cl^- transport from the electrolyte to the electrode. For the chlorination, Cl^- is a key reactant and should be supplied to the Ag surface from the electrolyte. When the NC layer is present on the surface, this shell serves as an additional barrier for the Cl^- transfer, and a larger driving force is thereby needed for the chlorination of the Ag electrode. However, mass transport of the reactant is not an influential governing factor for the rate of AgCl dechlorination, and thus, the NC has little effect on the reaction potential.

The Cl^--capture capacities of the four silver electrodes throughout the operations up to 500 cycles are summarized in

© 2025 The Author(s). ChemSusChem published by Wiley-VCH GmbH

18645648, 2025, 16, Downloaded from https://chemistry-europe.onlinelibrary.wiley.com/doi/10.1002/cssc.202500267 by Ewha Womans University Library, Wiley Online Library on [02/12/2025]. See the Terms and Conditions (https://onlinelibrary.wiley.com/terms-and-conditions) on Wiley Online Library for rules of use; OA articles are governed by the applicable Creative Commons License

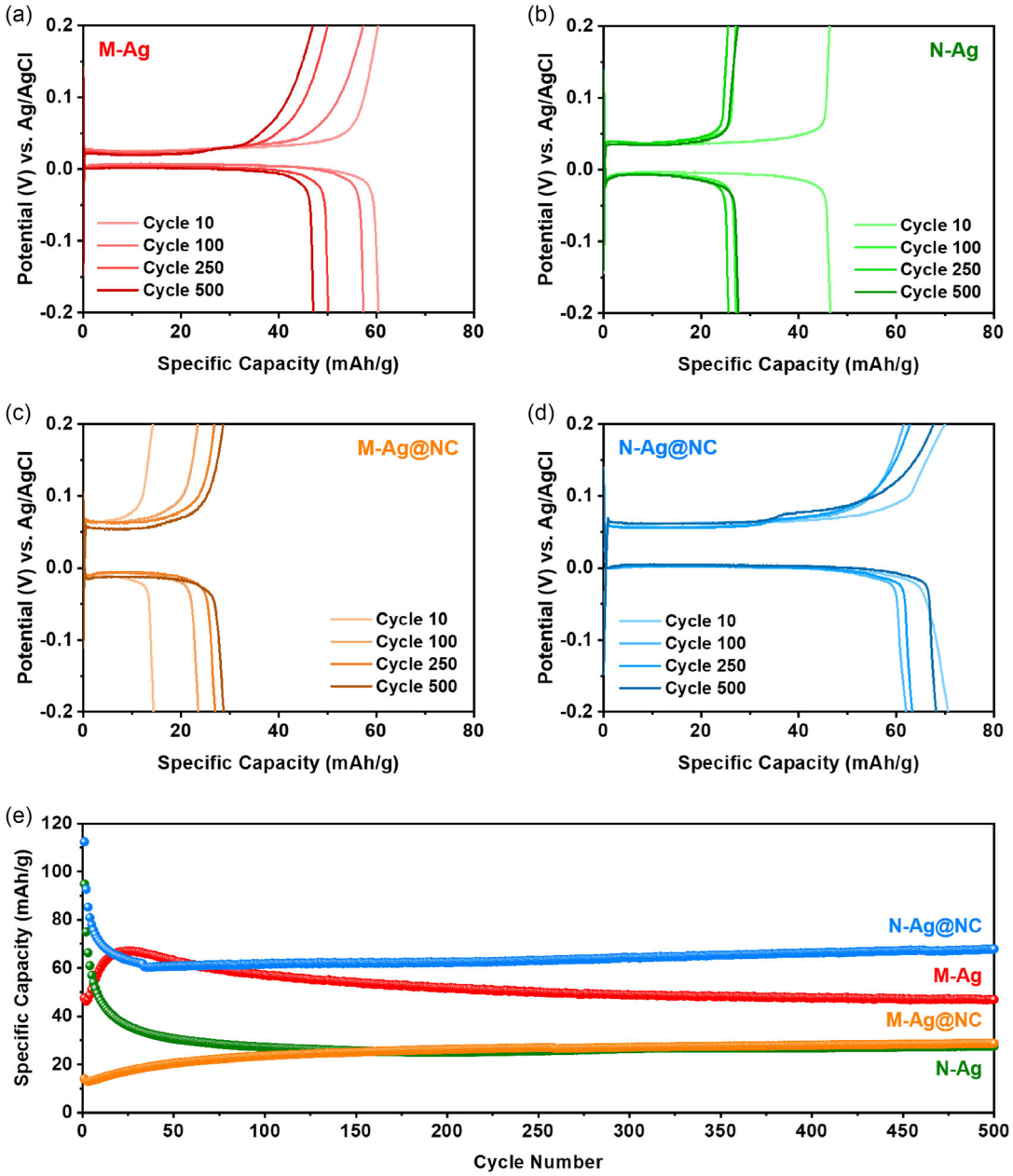


Figure 6. a–d) Charge–discharge profiles of the silver electrodes obtained by using 1 M NaCl solution as the electrolyte; (a) M-Ag, (b) N-Ag, (c) M-Ag@NC, and (d) N-Ag@NC. e) Chloride-capture capacities of the silver electrodes throughout the 500 cycle operations.

Figure 6e. These results could be understood as the desalination capabilities of the silver electrodes, given that the measurements were carried out using the aqueous NaCl solution as the electrolyte. At the initial cycles, nanosized particles (N-Ag and N-Ag@NC) showed superior performances, while the steep capacity decays were observable within ≈20 cycles. Continuous drop of performance was observable in the case of N-Ag, which eventually manifested the lowest Cl^--capture capacity from the ≈160th cycle until the end of the 500-cycle measurements. Microsized particles (M-Ag and M-Ag@NC) had relatively low capacities at the beginning, regardless of whether the silver particles were coated with NC or not. Meanwhile, the performance of M-Ag increased up to around the 25th cycle, which then started to fade gradually throughout the remaining cycles. This was attributable to the increased utilization of Ag (i.e., participation of the inner part of M-Ag particles in the chlorination), likely due to the development of porous structures during the initial cycles; detailed analysis using SEM will be introduced below.

Interestingly, M-Ag@NC manifested the lowest performance among the four Ag particles, and the initial capacity of M-Ag@NC was even lower than that of M-Ag by around three times. This substantial drop in performance was ascribed to the NC coating of silver, for this was the only difference between M-Ag and M-Ag@NC. Considering that the Ag chlorination accompanies volume expansion, the carbonaceous shell, which could enhance the overall conductivity and cyclic stability of the electrodes, can also

© 2025 The Author(s). ChemSusChem published by Wiley-VCH GmbH

1864564x, 2025, 16, Downloaded from https://chemistry-europe.onlinelibrary.wiley.com/doi/10.1002/cssc.202500267 by Ewha Womans University Library, Wiley Online Library on [02/12/2025]. See the Terms and Conditions (https://onlinelibrary.wiley.com/terms-and-conditions) on Wiley Online Library for rules of use; OA articles are governed by the applicable Creative Commons License

18645648, 2025, 16, Downloaded from https://chemistry-europe.onlinelibrary.wiley.com/doi/10.1002/cssc.202500267 by Ewha Womans University Library, Wiley Online Library on [02/12/2025]. See the Terms and Conditions (https://onlinelibrary.wiley.com/terms-and-conditions) on Wiley Online Library for rules of use; OA articles are governed by the applicable Creative Commons License

function as a mechanical barrier that suppresses the chlorination of Ag. For this reason, in the case of the NC-coated Ag particles, it is expected that a relatively small portion of Ag can participate in the reaction at the initial stage of operations. Moreover, there would be a larger chance of oxidative Ag dissolution, as the mechanical suppression of chlorination would result in the accumulation of positive charges (i.e., electron deficiency), which would possibly increase the local electrochemical potential more easily. Table S1, Supporting Information, shows the amounts of dissolved Ag during the 500-cycle operations, which were quantified by inductively coupled plasma-atomic emission spectroscopy (ICP-AES). It was noteworthy to find that the Ag dissolution was most significant in the case of M-Ag@NC among those four silver electrodes. Including those without carbon shells. This corroborates our discussion on the suppressed chlorination of Ag in M-Ag@NC, of which the carbon shell could serve as the mechanical barrier for the volume expansion.

On the other hand, the silver particles with the NC shells (both M-Ag@NC and N-Ag@NC) showed gradual increases in chloride-capture capacities as the cycle number increased. In the case of M-Ag@NC, there was a continuous rise in the capacity after the first few cycles. This observation could be explained by the development of voids within the shell (generated by Ag dissolution), as the empty space would result in the decreased mechanical-barrier effect. Rearrangements of silver within the carbonaceous matrix during the chlorination/dechlorination could also improve the utilization rate of Ag in M-Ag@NC. Regarding the N-Ag@NC, although there was a rapid capacity decay within ≈30 cycles, the performance increased in the remaining operation up to the 500th cycle, manifesting the highest Cl^--capture capacity among the four electrodes. ICP-AES result from N-Ag@NC shows that the dissolution of silver is substantially suppressed. The summary of the chloride-capture performances of the four silver electrodes and the comparison with the capacity and stability of silver-based electrodes in the literature are provided in Table S2 and S3, Supporting Information, respectively.

To further understand the behaviors of the silver particles during the cyclic operations, the morphologies of the electrodes were analyzed by using electron microscopes. **Figure 7** shows the SEM images of the four Ag electrodes (under chlorinated

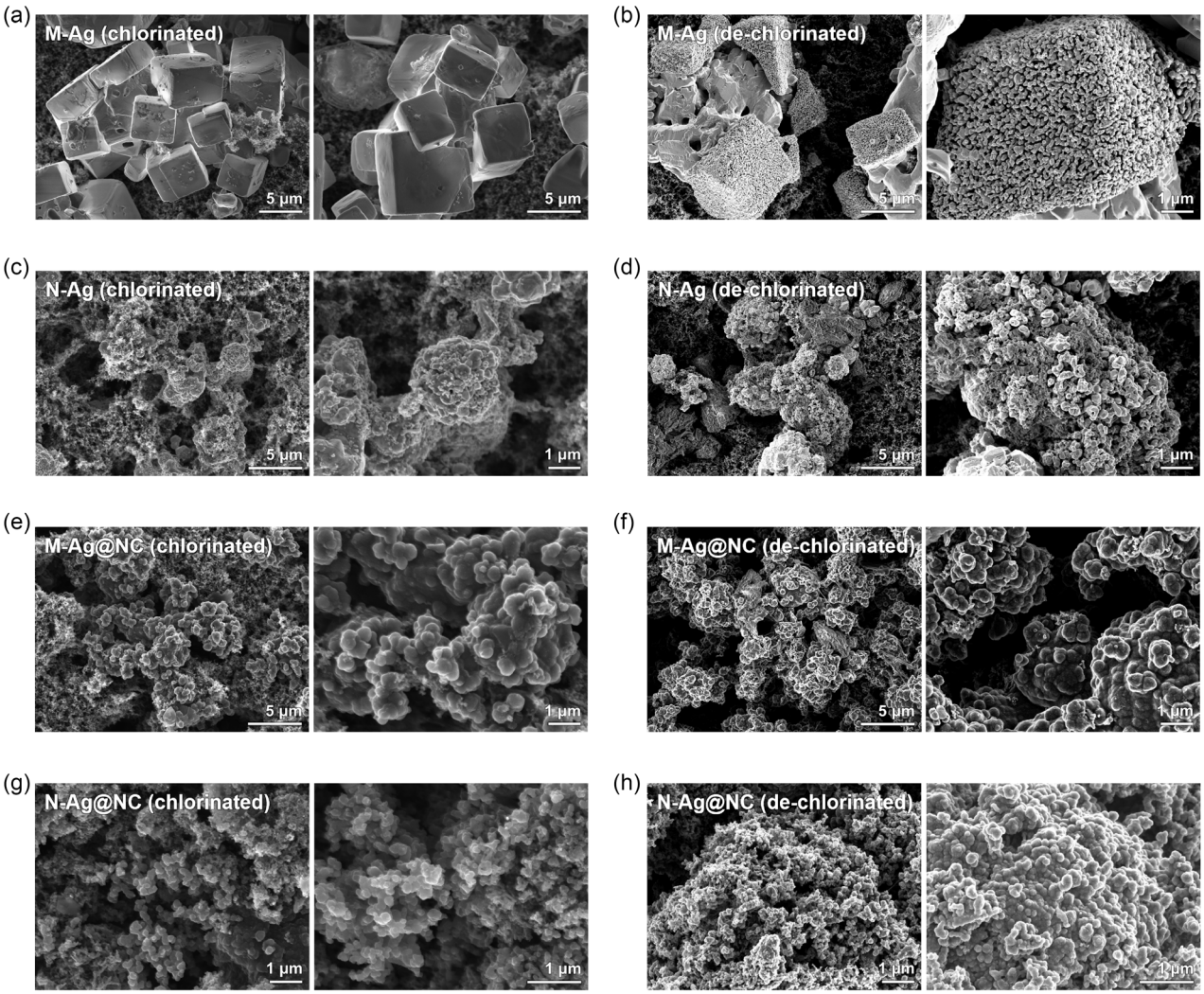


Figure 7. SEM images of a,c,e,g) chlorinated and b,d,f,h) dechlorinated silver electrodes after the 500 cycles of operations; (a,b) M-Ag, (c,d) N-Ag, (e,f) M-Ag@NC, and (g,h) N-Ag@NC.

© 2025 The Author(s). ChemSusChem published by Wiley-VCH GmbH

and dechlorinated conditions) after 500 cycles of operation. When compared with the structures of pristine silver particles displayed in Figure 4, it was clear that M-Ag and N-Ag underwent significant agglomerations during the operations (Figure 7a–d). The chlorinated M-Ag after the long-term cycles had the shape of agglomerated cuboids, whose size ranged from a few to tens of micrometers (Figure 7a). The structure also matched the cubic crystal structure of AgCl. Meanwhile, after the dechlorination of the 500-cycled M-Ag, the formation of nanopores throughout the cuboids was clearly observable (Figure 7b, additional SEM images are displayed in Figure S8, Supporting Information). This shows that a significant portion of silver in M-Ag can participate in the Cl^- capture and release quite effectively, though the increase of particle sizes would drop the capacities gradually. The development of nanoporous structure agrees with the increased performance during the initial stage (to around the 20th cycle) and the decent performance (being second among the tested silver particles) of M-Ag throughout the long-term operations.

There were no significant changes in the morphologies of the coated silver particles (Figure 7e–h). As the NC shells, which serve as the host for M-Ag@NC and N-Ag@NC, are unlikely to participate in Faradaic chlorination/dechlorination, the structure of the carbonaceous matrix would be retained throughout the operations. It was also noteworthy that there was no meaningful difference between the morphologies of the chlorinated and dechlorinated particles. This implies that the shells are contributing to the long-term stabilities, which is in line with the trend of Cl^--capture capacities summarized in Figure 6e. To understand how silver is located and distributed in the N-doped carbon, TEM images of chlorinated M-Ag@NC and N-Ag@NC after the 500 cycles were acquired (Figure S9, Supporting Information). Unlike the pristine particles, M-Ag@NC, which underwent the long-term chlorination/dechlorination cycles, had some empty space between the silver particles and the surrounding NC shells. This void could be attributed to the dissolution of silver during the operations. This actually agrees well with our interpretation on the significantly low capacity of M-Ag@NC, in which the NC shells could serve as the mechanical barrier for the volume expansion, suppressing the chlorination of silver while increasing the possibility for oxidative dissolution of Ag. Meanwhile, there was no significant changes in the overall structure of N-Ag@NC after the 500 cycles, though the redistribution of silver was detected from the decreased uniformity of silver nanoparticles embedded in N-doped carbons. The changes in the distribution of silver, which would possibly improve the transport of electrons and ions in the electrode and the electrolyte, respectively, seem to be a probable reason for the gradual capacity increase in the long-term operations.

Finally, chloride-capture performances of the silver electrodes were investigated in LiCl solutions to evaluate their feasibility in the electrochemical lithium recovery applications. Spinel-structured λ-MnO_2, which is known for its high Li^+ selectivity,[17,19,20] was used for the uptake of lithium ions. The electrodes were prepared by using $LiMn_2O_4$ as the active material based on the same procedure for the fabrication of Ag electrodes, followed by chemical delithiation by soaking the electrode in 1 M HCl(aq) solution for 2 h. Given that the separation of lithium ions is generally carried out using source waters with low Li^+ concentrations, 10 mM LiCl(aq) solution was used as the electrolyte. The measurements were performed using a flow-type electrochemical cell with the two-electrode configuration, wherein the space between the electrodes was minimized by using nonconductive nylon meshes (two sheets with a thickness of 100 μm each) as the spacer. For the operation, the potential window was 0.0 to +1.0 V versus Ag/AgCl, and the operation current densities were ±0.2 A g^{-1}. The flow rate of the electrolyte was 1 mL min^{-1}, and the ion concentrations were acquired by measuring the conductivity of the electrolyte at the outlet.

Figure 8a shows the chlorination capacities of the four silver electrodes throughout the 100 cycles of electrochemical lithium recovery processes. Due to the low ion concentration of the electrolyte, mass transfer of Cl^- was expected to be even more important, and the nanosized particles manifested superior initial performances; N-Ag without any barrier for the transport of Cl^- showed the highest capacity over the first 40 cycles. Both M-Ag and M-Ag@NC showed inferior capacities to the nanosized counterparts during the 100 cycles, and the NC shell resulted in decreased performance. However, N-doped carbon on the Ag surface did contribute to the enhanced stability; M-Ag@NC and N-Ag@NC showed enhanced capacity retention when

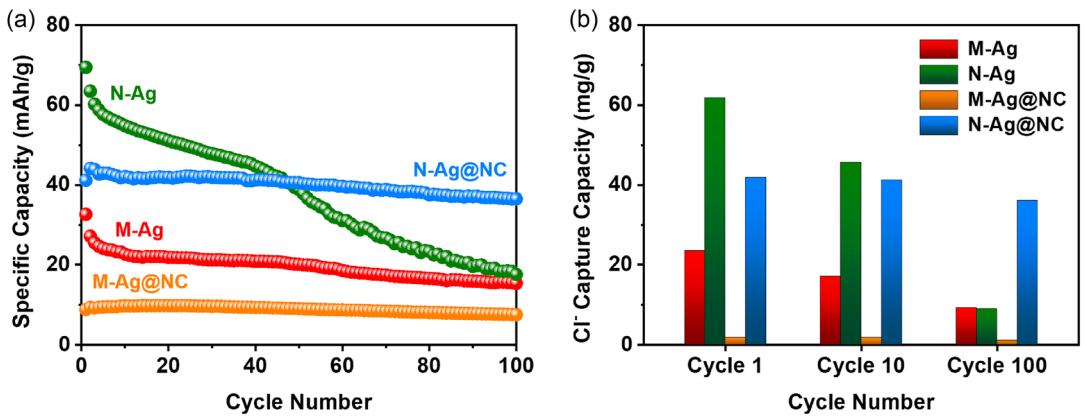


Figure 8. a) Chloride-capture capacities of the silver electrodes during 100 cycles of operation in 10 mM LiCl solution using λ-MnO_2 as the lithium-capturing counter electrode. b) The amounts of Cl^- captured at the 1st, 10th, and 100th cycles.

© 2025 The Author(s). ChemSusChem published by Wiley-VCH GmbH

18645648, 2025, 16, Downloaded from https://chemistry-europe.onlinelibrary.wiley.com/doi/10.1002/cssc.202500267 by Ewha Womans University Library, Wiley Online Library on [02/12/2025]. See the Terms and Conditions (https://onlinelibrary.wiley.com/terms-and-conditions) on Wiley Online Library for rules of use; OA articles are governed by the applicable Creative Commons License

compared with M-Ag and N-Ag, respectively. Moreover, N-Ag showed a rapid performance drop, and its capacity was around half that of N-Ag@NC, which retained 88.8% of its initial performance at the 100th cycle (82.7% retention from the highest-capacity cycle). The Cl^- concentrations at the outlet at the 1st, 10th, and 100th cycles measured by using a conductivity meter are displayed in Figure 8b. These results matched well with the capacities in Figure 8a, supporting the reliability of not only our measurements but also the robustness of the silver electrodes in the lithium recovery process; the Cl^- uptake by N-Ag@NC at the last cycle was 86.2% that of the first cycle.

3. Conclusions

In this study, nanosized silver particles with NC shells on the surface, or N-Ag@NC, were developed for electrochemical chloride capture in desalination and lithium recovery processes. Starting from the micrometer-scale commercial Ag, nanometer-scale AgCl particles were obtained by chlorination coupled with the reduction of iron cations. Then, polydopamine was introduced on the surface and was carbonized by thermal annealing. In the meantime, the first oxidation step in the dopamine polymerization process was coupled with the reduction of AgCl to Ag, resulting in the synthesis of metallic Ag nanoparticles coated with NC. These nanoparticles prepared by the coupling of reactions manifested excellent performance and robustness in chloride capture, verifying their feasibility for electrochemical desalination processes. We thoroughly analyzed structural changes of various silver particles (micro- and nanoscale silver particles with and without NC on the surface) after the long-term cyclic operations, which unveiled the advantages of the small particle size and the presence of carbonaceous shells. We additionally demonstrated the high capacity and stability of N-Ag@NC in electrochemical lithium recovery using a flow-type system, which corroborated the versatility of the coated silver nanoparticles in various chloride-capture applications. The enhanced performances of N-Ag@NC were achievable by the rational design, and the procedures used for the synthesis of N-Ag@NC, which involve coupling of reactions with favorable redox potentials, not only simplified but also improved the reliability of the whole process. For this reason, we believe that the strategies used in this work would provide significant insights for the development of electrode materials for various purposes, especially when designing the materials and their synthesis methods.

4. Experimental Section

Commercial silver particles with micrometer-scale sizes were purchased from Henqiu Technology, and other chemical reagents used in this study were purchased from Sigma-Aldrich. The morphologies of the silver particles and the electrodes were characterized by obtaining SEM and TEM images by using Carl Zeiss AURIGA and Jeol JEM-2100 F, respectively. TGA analysis was carried out by using TA Instruments SDT-Q600. High-resolution XRD patterns and XPS spectra were acquired at 9B and 10A2 beamlines of Pohang Accelerator Laboratory (PAL) in the Republic of Korea. The electrodes were prepared by doctor-blading of the slurry containing active materials, conducting agents, and polymeric binders in the ratio of 8:1:1 by weight. CV diagrams, charge–discharge profiles, and EIS spectra were obtained by using potentiostats (VersaSTAT3, Princeton Applied Research and VSP-3e, BioLogic) and a battery cycler (WBCS3000, WonATech), respectively. Shimadzu ICPS-8100 and PerkinElmer Optima 8300 were employed for the ICP-AES analysis. Horiba 3574-1°C was used to measure the conductivity. BET analysis was carried out by using MicrotracBel BELSORP-mini II.

Acknowledgements

This research work was supported by the National Research Foundation of Korea (NRF) funded by the Korean government (MSIT) through General Grant (no. RS-2023-00252746), Outstanding Young Scientist Grant (no. RS-2023-00211940), and Innovation Research Center (IRC) Grant (no. RS-2023-00261543). This work was also supported by the Institute for Basic Science (IBS) in the Republic of Korea (no. IBS-R006-A2) and by the Ewha Womans University Research Grant of 2023.

Conflict of Interest

The authors declare no conflict of interest.

Data Availability Statement

The data that support the findings of this study are available from the corresponding author upon reasonable request.

Keywords: chloride capture · desalination · electrochemistry · resource recoverives · silver

[1] M. A. Shannon, P. W. Bohn, M. Elimelech, J. G. Georgiadis, B. J. Mariñas, A. M. Mayes, *Nature* **2008**, *452*, 301.
[2] M. S. Diallo, M. R. Kotte, M. Cho, *Environ. Sci. Technol.* **2015**, *49*, 9390.
[3] H. M. Qiblawey, F. Banat, *Desalination* **2008**, *220*, 633.
[4] L. F. Greenlee, D. F. Lawler, B. D. Freeman, B. Marrot, P. Moulin, *Water Res.* **2009**, *43*, 2317.
[5] R. Chitrakar, H. Kanoh, Y. Miyai, K. Ooi, *Ind. Eng. Chem. Res.* **2001**, *40*, 2054.
[6] J. W. An, D. J. Kang, K. T. Tran, M. J. Kim, T. Lim, T. Tran, *Hydrometallurgy* **2012**, *117*, 64.
[7] X. Liu, S. Shanbhag, M. S. Mauter, *Curr. Opin. Chem. Eng.* **2019**, *25*, 67.
[8] P. Srimuk, X. Su, J. Yoon, D. Aurbach, V. Presser, *Nat. Rev. Mater.* **2020**, *5*, 517.
[9] Y. Liu, K. Wang, X. Xu, K. Eid, A. Moustafa, L. Pan, Y. Yamauchi, *ACS Nano* **2021**, *15*, 13924.
[10] H. Yoon, J. Lee, S. Kim, J. Yoon, *Sep. Purif. Technol.* **2019**, *215*, 190.
[11] Y. Qiu, C. Zhang, R. Zhang, Z. Liu, H. Yang, S. Qi, Y. Hou, G. Wen, J. Liu, D. Wang, *Green Energy Environ.* **2023**, *8*, 1488.
[12] Z. Liu, D. Wang, H. Yang, L. Feng, X. Xu, W. Si, Y. Hou, G. Wen, R. Zhang, J. Qiu, *Angew. Chem. Int. Ed.* **2024**, *136*, e202409204.
[13] M. Pasta, C. D. Wessells, Y. Cui, F. La Mantia, *Nano Lett.* **2012**, *12*, 839.
[14] X. Su, T. A. Hatton, *Phys. Chem. Chem. Phys.* **2017**, *19*, 23570.
[15] M. E. Suss, S. Porada, X. Sun, P. M. Biesheuvel, J. Yoon, V. Presser, *Energy Environ. Sci.* **2015**, *8*, 2296.
[16] M. Pasta, A. Battistel, F. La Mantia, *Energy Environ. Sci.* **2012**, *5*, 9487.
[17] J. Lee, S.-H. Yu, C. Kim, Y.-E. Sung, J. Yoon, *Phys. Chem. Chem. Phys.* **2013**, *15*, 7690.
[18] A. Battistel, M. S. Palagonia, D. Brogioli, F. La Mantia, R. Trócoli, *Adv. Mater.* **2020**, *32*, 1905440.

© 2025 The Author(s). ChemSusChem published by Wiley-VCH GmbH

1864564x, 2025, 16, Downloaded from https://chemistry-europe.onlinelibrary.wiley.com/doi/10.1002/cssc.202500267 by Ewha Womans University Library, Wiley Online Library on [02/12/2025]. See the Terms and Conditions (https://onlinelibrary.wiley.com/terms-and-conditions) on Wiley Online Library for rules of use; OA articles are governed by the applicable Creative Commons License

[19] L. Wu, C. Zhang, S. Kim, T. A. Hatton, H. Mo, T. D. Waite, *Water Res.* **2022**, *221*, 118822.
[20] S. Kim, J. Lee, J. S. Kang, K. Jo, S. Kim, Y.-E. Sung, J. Yoon, *Chemosphere* **2015**, *125*, 50.
[21] Y. Liu, C. Nie, X. Liu, X. Xu, Z. Sun, L. Pan, *RSC Adv.* **2015**, *5*, 15205.
[22] Z.-H. Huang, Z. Yang, F. Kang, M. Inagaki, *J. Mater. Chem. A* **2017**, *5*, 470.
[23] D. Kang, C. Huang, M. Ding, H. Y. Yang, *Desalination* **2024**, *586*, 117884.
[24] H. Yang, R. Zhang, Z. Liu, X. Xu, Y. Teng, M. Hou, G. Zhang, Y. Hou, G. Wen, D. Wang, *Chem. Eng. J.* **2024**, *501*, 157769.
[25] D.-H. Nam, K.-S. Choi, *J. Am. Chem. Soc.* **2017**, *139*, 11055.
[26] P. Srimuk, S. Husmann, V. Presser, *RSC Adv.* **2019**, *9*, 14849.
[27] K. Wang, Y. Liu, Z. Ding, Z. Chen, X. Xu, M. Wang, T. Lu, L. Pan, *Chem. Eng. J.* **2022**, *433*, 133578.
[28] Y. Liu, L. Wang, Q. Yao, X. Gao, X. Du, X. Dou, H. Zhu, X. Yuan, J. Xie, *Adv. Funct. Mater.* **2022**, *32*, 2110087.
[29] Y. Qiao, Y. Li, C. Wang, Q. Pan, B. Chen, Y. Wang, *ACS Sustainable Chem. Eng.* **2024**, *12*, 11692.
[30] J. Ahn, J. Lee, S. Kim, C. Kim, J. Lee, P. M. Biesheuvel, J. Yoon, *Desalination* **2020**, *476*, 114216.
[31] S. Kim, M. P. Nitsche, S. B. Rufer, J. R. Lake, K. K. Varanasi, T. A. Hatton, *Energy Environ. Sci.* **2023**, *16*, 2030.
[32] F. Chen, Y. Huang, L. Guo, M. Ding, H. Y. Yang, *Nanoscale* **2017**, *9*, 10101.
[33] Y. He, L. Huang, Y. Zhao, W. Yang, T. Hao, B. Wu, H. Deng, D. Wei, H. Wang, J. Luo, *Environ. Sci.: Nano* **2020**, *7*, 3007.
[34] L. Yan, B. Wu, Y. Zhao, J. A. Asare, H. Gang, D. Wei, Y. Cao, P. Chen, H. Wang, L. Huang, *Sep. Purif. Technol.* **2023**, *322*, 124210.
[35] Y. He, B. Wu, S. I. Alhassan, L. Yan, Y. Cao, D. Wei, B. Ouyang, P. Chen, T. Zhang, H. Wang, L. Huang, *Sep. Purif. Technol.* **2024**, *240*, 126564.
[36] Y. Cao, L. Yan, B. Wu, D. Wei, B. Ouyang, P. Chen, T. Zhang, J. A. Asare, Y. Jiang, Y. He, H. Wang, *Desalination* **2024**, *581*, 117603.
[37] M. Liang, L. Wang, V. Presser, X. Dai, F. Yu, J. Ma, *Adv. Sci.* **2020**, *7*, 2000621.
[38] D. Wei, B. Ouyang, Y. Cao, Y. Qing, P. Chen, T. Zhang, Y. He, L. Huang, C. Bao, H. Wang, *Chem. Eng. J.* **2024**, *500*, 157441.
[39] W. Kong, X. Lu, Y. Wang, K. Tan, C. Liu, J. Sun, M. Zhang, Y. Feng, *Small* **2025**, *21*, 2409342.
[40] B. Ma, J. Guo, W.-L. Dai, K. Fan, *Appl. Catal. B: Environ.* **2013**, *130*, 257.
[41] M. D. Hawley, S. V. Tatawawadi, S. Piekarski, R. N. Adams, *J. Am. Chem. Soc.* **1967**, *89*, 447.
[42] Y. Li, M. Liu, C. Xiang, Q. Xie, S. Yao, *Thin Solid Films* **2006**, *497*, 270.
[43] J.-L. Wang, B.-C. Li, Z.-J. Li, K.-F. Ren, L.-J. Jin, S.-M. Zhang, H. Chang, Y.-X. Sun, J. Ji, *Biomaterials* **2014**, *35*, 7679.
[44] L. C. Almeida, T. Frade, R. D. Correia, Y. Niu, G. Jin, J. P. Correia, A. S. Viana, *Sci. Rep.* **2021**, *11*, 2237.
[45] D. Y. Chung, S. W. Jun, G. Yoon, S. G. Kwon, D. Y. Shin, P. Seo, J. M. Yoo, H. Shin, Y.-H. Chung, H. Kim, B. S. Mun, K.-S. Lee, N.-S. Lee, S. J. Yoo, D.-H. Lim, K. Kang, Y.-E. Sung, T. Hyeon, *J. Am. Chem. Soc.* **2015**, *137*, 15478.
[46] D. Guo, R. Shibuya, C. Akiba, S. Saji, T. Kondo, J. Nakamura, *Science* **2016**, *351*, 361.
[47] J. S. Kang, S. Kim, D. Y. Chung, Y. J. Son, K. Jo, X. Su, M. J. Lee, H. Joo, T. A. Hatton, J. Yoon, Y.-E. Sung, *Adv. Funct. Mater.* **2020**, *30*, 1909387.

Manuscript received: February 7, 2025
Revised manuscript received: June 16, 2025
Version of record online: July 11, 2025

© 2025 The Author(s). ChemSusChem published by Wiley-VCH GmbH

1864564x, 2025, 16, Downloaded from https://chemistry-europe.onlinelibrary.wiley.com/doi/10.1002/cssc.202500267 by Ewha Womans University Library, Wiley Online Library on [02/12/2025]. See the Terms and Conditions (https://onlinelibrary.wiley.com/terms-and-conditions) on Wiley Online Library for rules of use; OA articles are governed by the applicable Creative Commons License